JMEPEG (2011) 20:839–845
DOI: 10.1007/s11665-010-9709-y

1059-9495/$19.00

Mechanical Properties and Welding Power of Friction Stirred AA2024-T35 Joints

H. Abd El-Hafez

(Submitted September 11, 2009; in revised form June 8, 2010)

This study is concerned with the effect of friction stir welding (FSW) parameters on the mechanical properties and the consumed welding power for AA2024-T35 joints. AA2024-T35 is friction stir welded at different welding speeds (16, 40, and 80 mm/min), rotation speed (900, 1120, and 1400 rpm), and two tool profiles (triangular and square). The welding power is measured and evaluated with two previously established models (O. Frigaad, O. Grong, and O.T. Midling, A Process Model for Friction Stir Welding of Age Hardening Aluminum Alloys, *Metall. Mater. Trans. A*, 2001, 32A, p 1189–1200; O.P. Heurtier, M.J. Jones, C. Desrayaud, J.H. Driver, F. Montheillet, and D. Allehaux, Mechanical and Thermal Modelling of Friction Stir Welding, *J. Mater. Process. Technol.*, 2006, 171, p 348–357). The tool profile as well as the welding speed show significant effect on the microstructure especially at lower welding speeds. The increase of the welding speed improves the mechanical properties for both tool profiles whereas it has an insignificant effect on the welding power. The square profile produces better mechanical properties and consumed more power, at 40 mm/min, than the triangular one. Moreover, the welding speed showed a weak effect on the welding power, but the need of power increased with the increase of the rotation speed. The measured power is found to be in agreement with the computed one through a theoretical work established by Heurtier et al. (Mechanical and Thermal Modelling of Friction Stir Welding, *J. Mater. Process. Technol.*, 2006, 171, p 348–357).

Keywords friction stir welding, rotation speed, welding power, welding speed

1. Introduction

The quality of friction stir processed (FSP) zone is controlled by the welding parameters (rotational speed, welding speed, and axial force) and by tool geometry (pin dimensions, pin profile, shoulder diameter, etc.). The optimization of all these parameters is very essential to obtain defect free joints. Elangovan and Balasubramanian (Ref 1) had studied the effect of welding speed and tool pin profile on FSP zone formation in AA2219 aluminum alloy. They found that the formation of defect free FSP zone is influenced by both welding speed and pin profile. The formation of defects and discontinuities are controlled by the above-mentioned parameters and these defects and discontinuities obviously influence the tensile properties of the friction stir welding (FSW) joints. Moreover, the joint fabricated using square pin profile at a certain welding speed of 0.76 mm/s exhibited maximum tensile strength, higher hardness, and finer grains in the FSP region compared to other joints.

The flow of the base material on the advancing side and the retreating side is different. The material on the retreating side never enters the rotational zone, while the material on the advancing side forms the fluidized bed near the pin and rotates around it (Ref 2). Figure 1 illustrates the FSW process (Ref 3).

H. Abd El-Hafez, Faculty of Engineering, Port Said University, 42523 Port Said, Egypt. Contact e-mail: abdelhafez1@gmail.com.

The welding tool left behind it many micro-pores when it moves forward along the welding line and at the same time, the tool filled each micro-pore. Hence, the FSW can be considered as micro-pores generation and disappearing procedure. Faster the welding speed is, larger is the pore. When welding and rotation speeds are constant, pores occur at small welding pressure (Ref 4).

In addition, Lee et al. (Ref 5) reported that the hardness of the weld nugget of FSW 6061Al at higher rotation rates was higher than that at lower rotation rates due to a higher density of spherical-shaped reprecipitates. However, when both rotation rate and welding speed changed, it was hard to evaluate quantitatively the parameter dependence of the thermal input and mechanical properties (Ref 6). For the precipitation-hardened aluminum alloys, FSW creates a softened region in the heat affected zone (HAZ) that has the lowest hardness within the entire weld, due to significant dissolution/coarsening of the precipitates during the FSW thermal cycle (Ref 7, 8). Thus, the HAZ exhibits the lowest hardness and strength, and the fracture occurs usually in the HAZ (Ref 6, 8). Therefore, the hardness profile of the FSW aluminum alloy joint is a direct indicator of microstructural evolution during FSW as concluded by Liu and Ma (Ref 9).

The development of mathematical models can greatly contribute to better understanding any industrial process, particularly FSW. A validated model has the potential to produce reliable information about the deformation and mixing patterns that are important when designing FSW tools, and thus should be capable of producing welds free of defects and voids (Ref 10).

Although several numerical models of FSW have been developed for the calculation of heat generation rate (Ref 11-13), heat transfer, and materials flow (Ref 2, 13-15), their testing

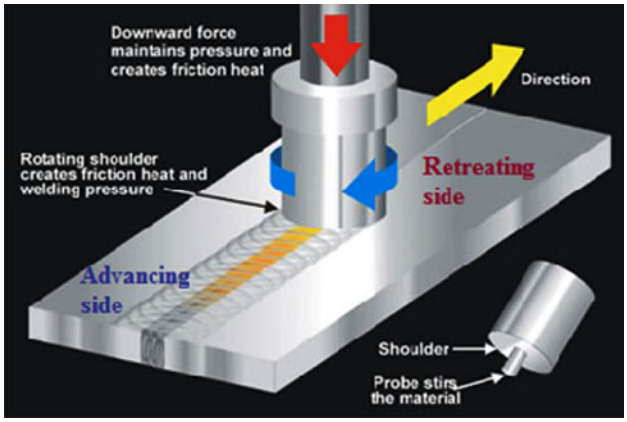

Fig. 1 Schematic drawing of the friction stir welding process (Ref 3)

has, for the most part, been limited to comparison of the numerically predicted temperature versus time plots with the corresponding experimental data. A rigorous validation of numerical models must include examination of model capabilities to predict several important features of FSW. Features such as the torque and the power needed for welding, and the geometry of the stir zone as a function of important welding variables over a wide range of values are considered. However, new researches evaluated by Arora et al. (Ref 16) and El-Domiaty and Abd El-Hafez (Ref 17) studied the power requirement for FSW through modeling. They concluded that the welding speed has neglected the effect on the welding power, whereas the increase of the rotation speed increased the welding power because it became easier for the material to flow at higher temperatures and strain rates.

Zhang and Zhang (Ref 18-21) established other thermomechanical models. They concluded that when the welding speed became higher, the rotating speed must be increased simultaneously to avoid any possible welding defects such as voids. The simultaneous increase of the rotating and the welding speeds can lead to the increase of the residual stresses. The maximum temperature in the FSW process can be increased with the increase of the rotating speed. Furthermore, the power needed for FSW was increased with the increase of the rotating and the welding speeds.

In this study, the microstructure, the hardness distribution, and the tensile properties of AA2024-T35 plates; friction stir welded using triangular and square tool profiles at different rotation and welding speeds, were investigated. In addition, the consumed welding power was measured and evaluated with two models established elsewhere (Ref 22, 23).

2. Experimental Work

The base alloy, used in this study, is the hot-rolled aluminum alloy 2024-T35, 5-mm thickness, 50-mm width, and 200-mm length. The chemical composition of AA2024-T35 is shown in Table 1. Two plates were friction stir welded normal to the rolling direction at different welding speeds (16, 40, and 80 mm/min) and at different rotation speeds (900, 1120, and 1400 rpm). An equal welding force can be obtained by

Table 1 The chemical composition of Al-alloy 2024-T35

Chemical composition, wt.%							
Si	Fe	Cu	Mn	Mg	Cr	Zn	Al
0.50	0.37	4.4	0.6	1.5	0.12	0.25	Bal

controlling the plunge depth of the welding tool, since the friction stir zone of all the specimens has the same thickness. Other FSW process parameters are kept constant.

According to the previous studies (Ref 21, 23, 24), triangular and square tool profiles are chosen to carry out the FS-joints in this study.

Non-consumable tools made of X40 CrMoV 5 1 have been used to fabricate the joints. The tools are treated by hardening and tempering processes, where the hardness is increased to 54 HRC. The tools have a concave shoulder of 20-mm diameter with slope of 10° and the triangle and square pin profiles of 5-mm root diameter and 4.8-mm length were used.

The initial joint configuration is obtained by securing the plates in position using mechanical clamps. Single pass welding procedure has been used to fabricate the joints.

The electrical power, during welding processes, is measured using clamp-meter. The power (q) is calculated using the following equation for three-phase (Ref 25):

$$q = \sqrt{3}\, VI \cos\theta \ (\mathrm{W}), \qquad \text{(Eq 1)}$$

where V is the voltage, I the current in ampere, and cos θ is the power factor. The voltage (V) was constant around 380 V and the power factor is 0.8. Therefore, the power calculations depend only on the current value.

After welding, the FSW samples were cross-sectioned perpendicular to the welding direction for microstructural examinations by optical microscopy, hardness measurement, and tensile test. Three tensile specimens are tested at each condition and their average represents one point data.

Vickers microhardness distribution is measured from the weld center on both retreating and advancing sides. The hardness measured across the joint has been carried out using the Vickers microhardness-testing machine with an applied load of 0.5 kg load.

3. Results and Discussion

3.1 Microstructural Characteristics

Macrostructure shows that, at 40 mm/min, the weld is perfect and no obvious defects produced. The materials are stirred, combined sufficiently and the weld is completely filled. On the other hand, voids are noticed near the weld root when the welding speed is 80 mm/min, as shown in Fig. 2(a). The voids produced near the welding line can be considered as normal criteria; in fact, additional superplasticity was needed to fill the gap of the base metal (Ref 4).

Figure 2(b) and (c) presents micrographs showing the evaluation of 2024-T35 microstructure, carried out at 40 mm/min for square profile, in FS-region. Figure 2(b) shows the microstructure under the tool shoulder whereas the bottom of the specimen, near the weld root, is shown in Fig. 2(c). The two figures have different distribution of the white and dark zones

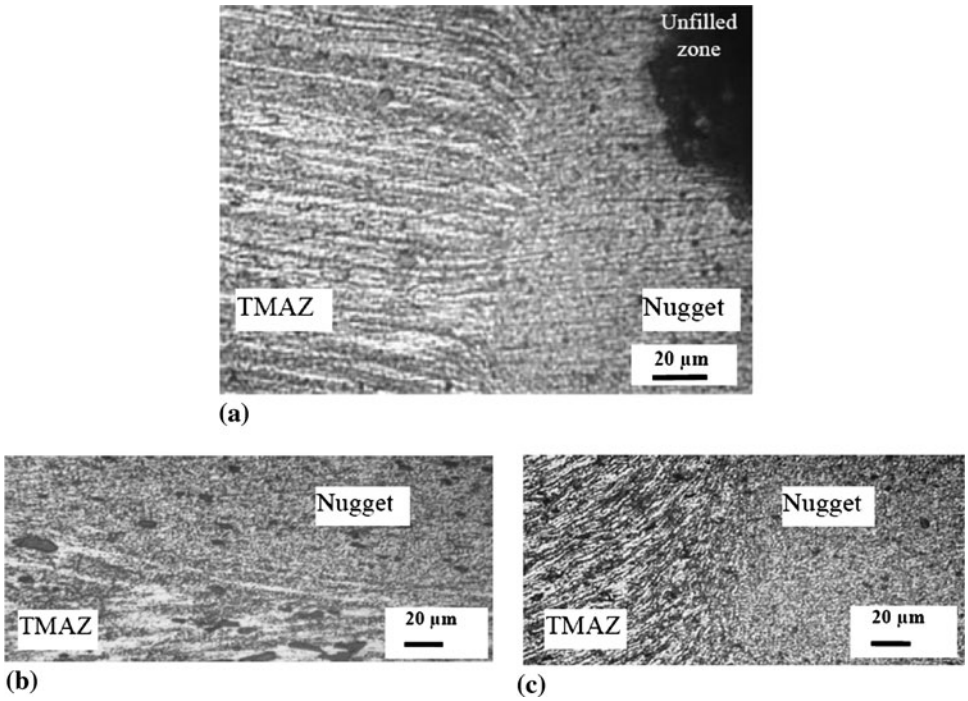

Fig. 2 Micrographs of the microstructure of AA2024-T35. (a) Incomplete filling near the weld root at the weld line (80 mm/min, 1120 rpm), (b) under the shoulder, and (c) bottom of the specimen (near the weld root) (40 mm/min, 1120 rpm)

(bands), which may be attributed to the higher heat generated near the tool shoulder where coarser grains can be noticed in the thermal mechanical affected zone (TMAZ). In addition, the $CuAl_2$ phase (dark area) is distributed in both nugget and TMAZ.

However, Sutton et al. (Ref 26) proved that the spacing between the dark bands would decrease as the welding speed is reduced. Smaller band spacing should result in a more homogeneous structure within the weld. They demonstrated, using EDX analysis, that the dark particles contain higher concentrations of Cu, Fe, Mg, and Mn than the surrounding white material.

From the microstructure analysis, it can be inferred that the formation of defect free FSP zone is a function of the used tool profile and the applied welding speeds.

3.2 Hardness Distributions

Hardness distribution on the transverse cross-section of the joints at different welding speeds and the rotation speed of 1120 rpm for the square profile is shown in Fig. 3.

Minimum hardness appeared in the HAZ and its value increased with the increase of the welding speed. The softened zones existing on both sides of the HAZ were shifted toward the welding center line as the welding speed increased (Ref 27). The lower hardness values of the HAZ can be attributed mainly to the absence of the coarsened precipitates. Also, the softened area is narrower at the higher welding speed than that for the lower welding speeds (Ref 28). The welding speed of 40 mm/min has the same trend on advanced side but on the retreating side, the hardness is higher than the other speeds in the soft zone.

Results from metallurgical and hardness measurements show that the FSW process can create a segregated banded

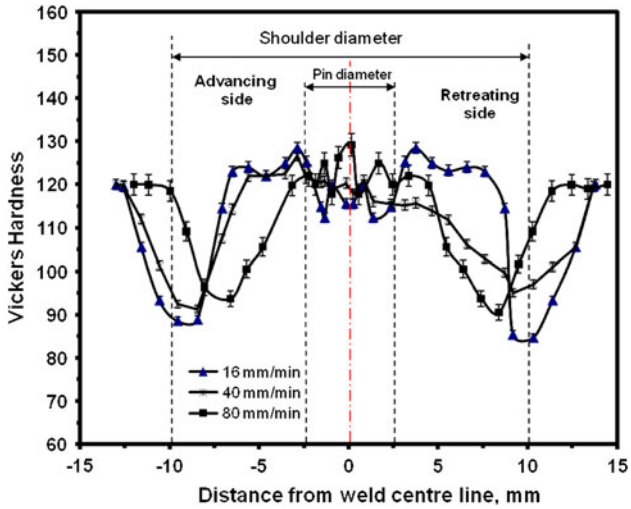

Fig. 3 Hardness distribution, at different welding speeds, for square profile joints

microstructure consisting of alternating hard particle-rich (dark areas) and hard particle-poor (white areas) regions.

3.3 Fracture Behavior

The fracture behavior of the tensile specimens shows two trends. The first one where the fracture takes place at the end of tool shoulder usually at the retreating side, as shown in Fig. 4(a). The second fracture path is at the weld line (nugget), as shown in Fig. 4(b).

Most joints are fractured at the retreating side, which is due to variation in the temperature distribution and the flow of the

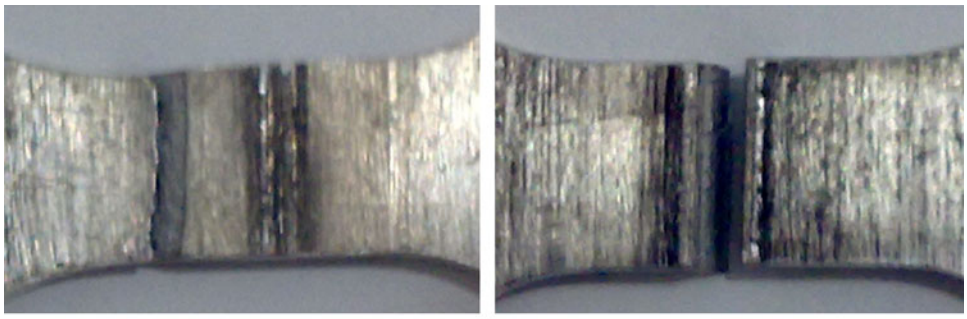

Fig. 4 Macrographs of the fracture path of the FSW tensile specimens. (a) Tensile fracture at the retreating side and (b) tensile fracture through the weld nugget (weld line)

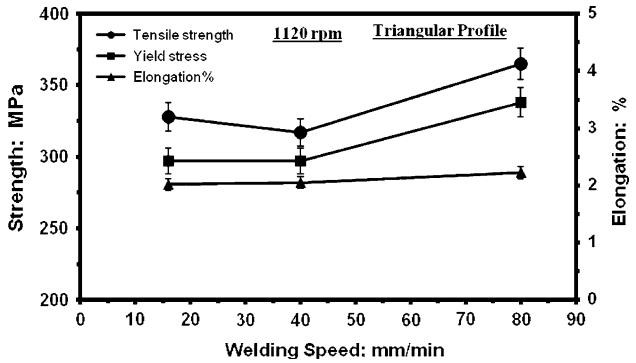

Fig. 5 Effect of welding speed on the mechanical properties of the FS-joints using triangular profile

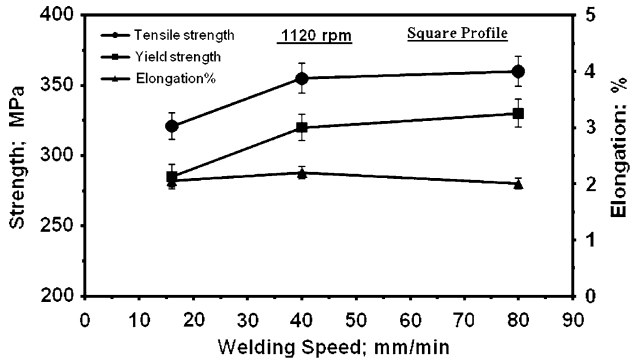

Fig. 6 Effect of welding speed on the mechanical properties of the FS-joints using square profile

material in the weld zone with corresponding hardness distribution and strained region. Moreover, due to different deformation of various zones, the strain becomes localized, which induces constraint. Meanwhile the fracture occurs, as well, where the strain localization is the highest. For this alloy, the retreating side of the weld zone has been found to be the major fracture site where strain localization occurred (Ref 1, 29).

3.4 Tensile Results

Figure 5 illustrates the effect of the welding speed on the yield stress, the tensile strength, and the elongation percent for the fabricated triangular profile joints. The effect of the welding speed was investigated at a constant rotation speed of 1120 rpm. The results show a noticeable improvement of the mechanical properties at the welding speed range from 40 to 80 mm/min but the increase of welding speed from 16 to 40 mm/min has no effect on the tensile properties. The improved mechanical properties at the welding speed of 80 mm/min may be attributed to the more homogeneity of the weld nugget and less pores, which results in sound joints.

Also, the results of the square profile with the aforementioned parameters are illustrated in Fig. 6. One can notice that for the increase of the welding speed from 16 to 40 mm/min, the yield strength as well as the tensile strength increase and remain almost steady above this speed.

The tensile properties and fracture locations depend mainly on the welding defects and hardness of the joint. When the joints are free from defects, their tensile properties are controlled by hardness and fracture occurred in the HAZ on the side that show minimum hardness (Ref 27). These results show better properties at 40 mm/min and this may be due to the sufficient heat generation to fill the pores in time.

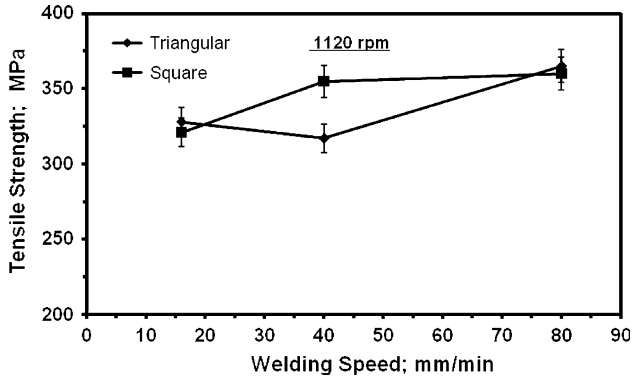

Fig. 7 Tool profile and the welding speed effects on the FS-joints strength

Lower welding speed resulted in higher temperature and slower cooling rate in the weld zone, which causes grain growth and severe clustering of $CuAl_2$ precipitates (Ref 1, 30).

The effect of the tool profile on the tensile strength is illustrated in Fig. 7. Insignificant effect of the tool profile at low welding speed is noticed. At higher welding speed of 40 mm/min,

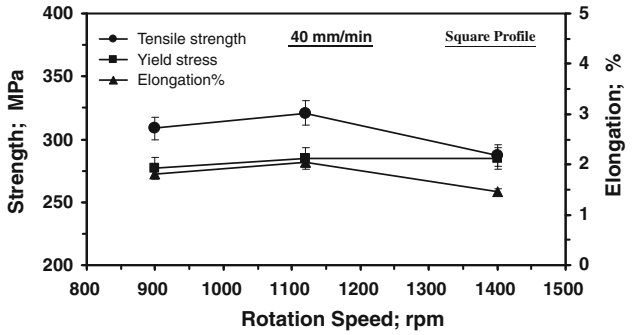

Fig. 8 Mechanical properties of AA2424-T35 FS-joints at different rotation speeds

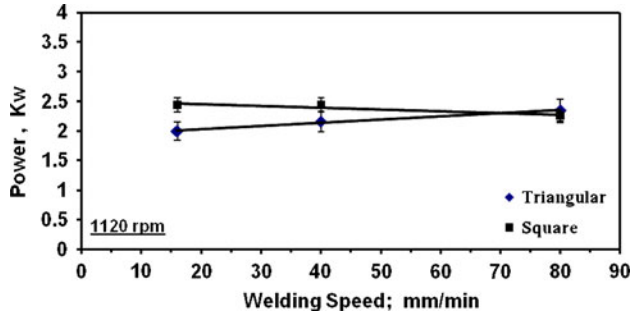

Fig. 9 Effect of welding speed and tool profile on the welding power

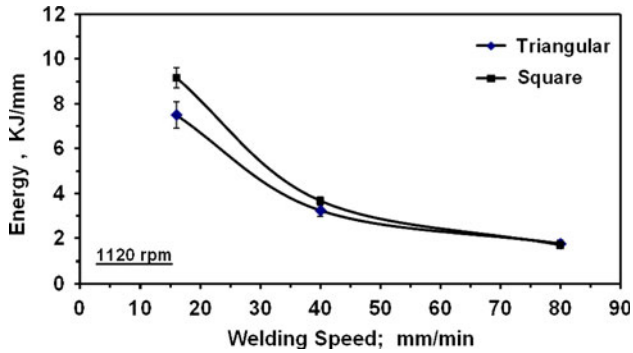

Fig. 10 Effect of welding speed and tool profile on the energy

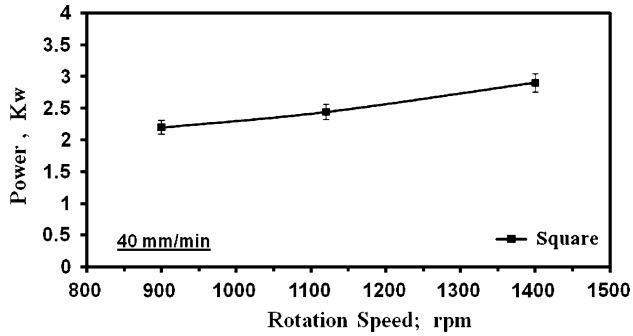

Fig. 11 Welding power and rotation speed for square tool profile

the square profile achieves higher strength compared to the triangular one. Otherwise, an improvement for the triangular profile is noticed with the increasing of the welding speed to 80 mm/min, meanwhile this speed has a neglected effect on the square profile. Besides, at 80 mm/min, the tool profile has a weak effect on the strength.

However, it is clear that the welding speed of 40 mm/min can be considered as a critical speed for both profiles. The square profile has a sufficient heat generation whereas the triangular one achieves this heat at higher speed of 80 mm/min. The achieved higher strength using the square profile at 40 mm/min may be due to the produced higher pulses/s than that produced by the triangular one. The higher number of pulsating action produces finer grained microstructure with uniformly distributed precipitates ($CuAl_2$) and in turn yields higher strength and hardness (Ref 1, 28). Moreover, the behavior of the strength at 80 mm/min for the different tool profiles may be attributed to the stirring effect of the welding tool, which becomes weaker.

Otherwise, as the square profile achieved best properties, the effect of the rotation speed on the mechanical properties of the FS-joints is carried out, using square profile, at a constant welding speed of 40 mm/min. Figure 8 shows that the strength as well as the elongation percent has slight improvement at 1120 rpm, while the yield strength has neglected changes. The improvement of the mechanical properties at 1120 rpm may be associated with good stirring action along with uniformly distributed precipitates ($CuAl_2$). On the other hand, the strength has the lowest value at a high rotation speed of 1400 rpm that can be attributed to the increase of pores in the nugget zone (Ref 4, 18-21).

3.5 Welding Power

Figure 9 illustrates the measured welding power affected by different welding parameters. The variation of the welding speed does not significantly affect the power needed for FSW where the plastic deformation, due to the temperature rise, is increased with the increase of the welding speed (Ref 21, 31). Otherwise, the square tool profile needs more power than the triangular one at lower welding speed, which may be a result of the excess of pulses number per unit time than the triangular profile. However, by increasing the welding speed to 40 mm/min, the power difference occurred by tool profile can be neglected which is eliminated at higher welding speed of 80 mm/min.

The effect of the tool profile on the needed power decreases with the increase of the welding speed because when the welding speed is high, the stirring effect of the welding tool profile becomes weaker, which is the reason for the occurrence of the weld flow (Ref 21).

The energy is computed through dividing the power by the welding speed and the results were plotted in Fig. 10. The energy per unit length decreases with the increase of the welding speed since the energy is inversely proportional to the welding speed (Ref 16).

Otherwise, the effect of the rotation speed on the welding power for the square profile is illustrated in Fig. 11. The welding power needed for FSW is increased significantly with the increase of the rotation speed. Increasing the rotation speed increases the power input to the weld, while the welding speed had little impact (Ref 20, 32).

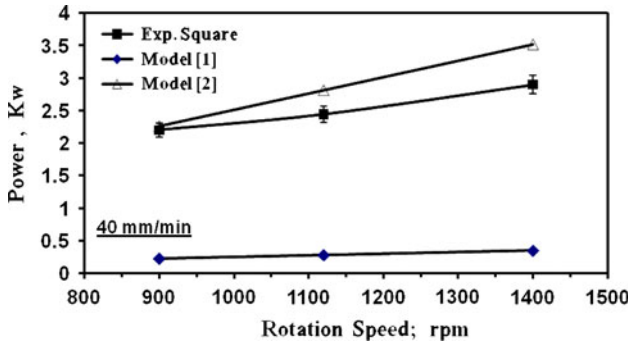

Fig. 12 Comparison between the experimental and theoretical results of the welding power at different rotation speeds

Many researchers have established different models to compute the welding power needed for FSW. In the present study, two of those models are used to assess the experimental measurements of the consumed power (q). These models are shown in Eq 2 Frigaad et al. (Ref 22) and Eq 3 Heurtier et al. (Ref 23).

$$q = \frac{4\pi^2}{3}\mu P\omega R^3 \text{ (W)} \qquad \text{(Eq 2)}$$

$$q = \frac{2\pi}{3}\mu P\omega R_S^3 \text{ (W)}, \qquad \text{(Eq 3)}$$

where μ is the friction coefficient, P is the pressure (Pa), ω is the tool angular speed (rad/s), R_S is the tool shoulder radius, and R is the pin radius. In fact, there is no experimental work done for the determination of the friction coefficient on the tool-plate interface until now. Zhang and Zhang (Ref 19) reported that the predicted temperature is very similar to the experimental measurement when the friction coefficient is taken as 0.3. Hence, this value is also adopted in the current work. The pressure P equals the force divided by the shoulder area, whereas the measured force by Elangovan and Balasubramanian (Ref 1), 12 KN for AA2219, is used in this study.

Figure 12 shows a comparison between the experimental and computed results at different rotation speeds. In general, it is clear that the power increases, linearly, with the increase of the rotation speed. Furthermore, the measured power is in good correlation with the theoretical results calculated from the second model established by Heurtier et al. (Ref 23). This correlation is excellent at the lower rotation speed of 900 rpm. For higher values of rotation speed, the power calculated from the model exceeds the measured values. The divergence between the two values increases as the rotation speed increases. This divergence could be attributed to the increase of the generated heat or to the sliding between the tool and the metal, or even due to other parameters might not be considered by Heurtier et al. (Ref 23).

4. Conclusion

A series of controlled friction stir welds have been manufactured using 5-mm thick, 2024-T35 aluminum rolled sheet material. Metallurgical investigation, hardness test, and tensile test results, as well as the measured welding power values show that:

1. The welding speed has a noticeable effect on the hardness distribution. As the welding speed increases, the hardness of the softened HAZ increases and the softened HAZ is shifted toward the weld line. Moreover, the hardness distribution affects the fracture path, which occurs usually in the softened zone.
2. The obtained tensile strength at a high welding speed of 80 mm/min using the triangular tool profile can be achieved at a lower welding speed of 40 mm/min in case of the square tool profile.
3. Increasing the rotation speed increases the consumed welding power, while the welding speed has a little effect on the consumed power.
4. The measured power agrees with corresponding values calculated using a model established by Heurtier et al. (Ref 23), especially at lower rotation speed. The computed power as well as the measured one has a linear relation with the rotation speed. At higher speeds, the theoretical results exceed the experimental results. Such deviation could be due to the increase of slipping between the tool and the metal at higher rotation speed, or due to a possible lack of the model-assumptions accuracy.

References

1. K. Elangovan and V. Balasubramanian, Influences of Tool Pin Profile and Welding Speed on the Formation of Friction Stir Processing Zone in AA2219 Aluminum Alloy, *Mater. Sci. Eng. A*, 2007, **459**(1–2), p 7–18
2. H.W. Zhang, Z. Zhang, and J.T. Chen, The Finite Element Simulation of the Friction Stir Welding Process, *Metall. Mater. Trans. A*, 2005, **403**, p 305–316
3. http://www.esabna.com/us/en/education/knowledge/images/FrictionStirWeldingChart.jpg, 7 Dec. 2009
4. H. Zhang, S.B. Lin, L. Wu, J.C. Feng, and Sh.L. Ma, Defects Formation Procedure and Mathematic Model for Defect Free Friction Stir Welding of Magnesium Alloy, *Mater. Des.*, 2006, **27**, p 805–809
5. W.B. Lee, Y.M. Yeon, and S.B. Jung, Mechanical Properties Related to Microstructural Variation of 6061 Al Alloy Joints by Friction Stir Welding, *Mater. Trans.*, 2004, **45**(6061), p 1700–1705
6. S.R. Ren, Z.Y. Ma, and L.Q. Chen, Effect of Welding Parameters on Tensile Properties and Fracture Behavior of Friction Stir Welded A-Mg-Si alloy, *Scr. Mater.*, 2007, **56**, p 69–72
7. S. Lim, S. Kim, C.G. Lee, and S. Kim, Tensile Behavior of Friction-Stir-Welded Al 6061-T651, *Metall. Mater. Trans. A*, 2004, **35A**, p 2829–2835
8. R.S. Mishra and Z.Y. Ma, Friction Stir Welding and Processing, *Mater. Sci. Eng. R*, 2005, **50**, p 1–78
9. F.C. Liu and Z.Y. Ma, Influence of Tool Dimension and Welding Parameters on Microstructure and Mechanical Properties of Friction-Stir-Welded 6061-T651 Aluminum Alloy, *Metall. Mater. Trans. A*, 2008, **39A**, p 2378–2388
10. P. Vilac, L. Quintino, and J.F. dos Santos, Analytical Thermal Model for Friction Stir Welding, *J. Mater. Process. Technol.*, 2005, **169**, p 452–465
11. M.Z.H. Khandkar, J.A. Khan, and A.P. Reynolds, Prediction of Temperature Distribution and Thermal History During Friction Stir Welding: An Input Torque Based Model, *Sci. Technol. Weld. Join.*, 2003, **8**(3), p 165–174
12. H. Schmidt, J. Hattel, and J. Wert, An Analytical Model for the Heat Generation in Friction Stir Welding, *Model. Simul. Mater. Sci. Eng.*, 2004, **12**, p 143–157
13. R. Nandan, T.J. Lienert, and T. DebRoy, Toward Reliable Calculations of Heat and Plastic Flow During Friction Stir Welding of Ti-6Al-4V Alloy, *Int. J. Mater. Res.*, 2008, **99**(4), p 434–444
14. R. Nandan, G.G. Roy, T.J. Lienert, and T. DebRoy, Numerical Modelling of 3D Plastic Flow and Heat Transfer During Friction Stir

Welding of Stainless Steel, *Sci. Technol. Weld. Join.*, 2006, **11**(5), p 526–537
15. R. Nandan, G.G. Roy, T.J. Lienert, and T. DebRoy, Three-Dimensional Heat and Material Flow During Friction Stir Welding of Mild Steel, *Acta Mater.*, 2007, **55**(3), p 883–895
16. A. Arora, R. Nandan, A.P. Reynolds, and T. DebRoy, Torque, Power Requirement and Stir Zone Geometry in Friction Stir Welding Through Modeling and Experiments, *Scr. Mater.*, 2009, **60**, p 13–16
17. A. El-Domiaty and H. Abd El-Hafez, An Energy Model for Friction Stir Welding, *Mater. Sci. Technol. Assoc. Iron Steel Technol.*, 2007, **3**, p 1709–1721
18. Z. Zhang and H.W. Zhang, Numerical Studies on the Effect of Axial Pressure in Friction Stir Welding, *Sci. Technol. Weld. Join.*, 2007, **12**, p 226–248
19. Z. Zhang and H.W. Zhang, A Fully Coupled Thermo-Mechanical Model of Friction Stir Welding, *Int. J. Adv. Manuf. Technol.*, 2008, **37**, p 279–293
20. Z. Zhang and H.W. Zhang, Numerical Studies on Controlling of Process Parameters in Friction Stir Welding, *J. Mater. Process. Technol.*, 2009, **209**, p 241–270
21. Z. Zhang and H.W. Zhang, Numerical Studies on the Effect of Transverse Speed in Friction Stir Welding, *Mater. Des.*, 2009, **30**, p 900–907
22. O. Frigaad, O. Grong, and O.T. Midling, A Process Model for Friction Stir Welding of Age Hardening Aluminum Alloys, *Metall. Mater. Trans. A*, 2001, **32A**, p 1189–1200
23. O.P. Heurtier, M.J. Jones, C. Desrayaud, J.H. Driver, F. Montheillet, and D. Allehaux, Mechanical and Thermal Modelling of Friction Stir Welding, *J. Mater. Process. Technol.*, 2006, **171**, p 348–357
24. G. Abd El-Nasser, A. El-Bagdady, and H. Abd El-Hafez, Effect of the Friction Stir Welding Parameters on the Mechanical Properties of Al 5083 Joint, *Al-Azahar Eng. 9th Int. Conf.*, 12–14 April 2007, Cairo, Egypt, p 356–367
25. C.K. Alexander and M.N.O. Sadiku, *Fundamentals of Electric Circuits*, 2nd ed., Chap. 12, Mc-Graw-Hill, 2000
26. M.A. Sutton, B. Yang, A.P. Reynolds, and R. Taylor, Microstructural Studies of Friction Stir Welds in 2024-T3 Aluminum, *Mater. Sci. Eng.*, 2002, **A323**, p 160–166
27. S.A. Khodir and T. Shibayanagi, Friction Stir Welding of Dissimilar AA2024 and AA7075 Aluminum Alloys, *Mater. Sci. Eng. B*, 2008, **148**(1–3), p 82–87
28. K. Elangovan, V. Balasubramanian, and S. Babu, Predicting Tensile Strength of Friction Stir Welded AA6061 Aluminium Alloy Joints by a Mathematical Model, *Mater. Des.*, 2009, **30**, p 188–193
29. C. S. Babu, A.S. El-Gizawy, and A. Sherif, Characterization of Friction Stir Welding Process Behaviour Using Numerical and Physical Modeling Techniques, *Proc. of the 9th Int. Conf. Mech. Des. Prod. (MDP-9)*, 8–10 Jan 2008, Cairo, Egypt, p 517–530
30. W.B. Lee, Y.M. Yeon, and S.B. Jung, Evaluation of the Microstructure and Mechanical Properties of Friction Stir Welded 6005 Aluminum Alloy, *Mater. Sci. Technol.*, 2003, **19**, p 1513–1518
31. H. Atharifar, D. Lin, and R. Kovacevic, Numerical and Experimental Investigations on the Loads Carried by the Tool During Friction Stir Welding, *J. Mater. Eng. Perform.*, 2008, **18**, p 339–350
32. P.A. Colegrove and H.R. Shercliff, 3-Dimensional CFD Modelling of Flow Round a Threaded Friction Stir Welding Tool Profile, *J. Mater. Process Technol.*, 2005, **169**, p 320–327